Національна академія наук України

ІНСТИТУТ ФІЗИКИ КОНДЕНСОВАНИХ СИСТЕМ

ICMP–24–03E

M. Parymuda, T. Krokhmalskii, O. Derzhko

PRELIMINARIES ON THERMODYNAMICS
OF HYPERKAGOME-LATTICE
$S = 1/2$ HEISENBERG FERROMAGNET

ЛЬВІВ

УДК: 537.9; 537.622

PACS: 75.10.-b

Попередні результати стосовно термодинаміки $S = 1/2$ феромагнетика Гайзенберга на гратці гіперкагоме

М. Паримуда, Т. Крохмальський, О. Держко

Анотація. $S = 1/2$ феромагнетик Гайзенберга на гратці гіперкагоме вивчається кількома методами (лінійна теорія спінових хвиль, двочасові температурні функції Гріна, високотемпературні розвинення та симуляції методом квантового Монте Карло) щоб дослідити вплив геометрії гратки на властивості системи при скінчених температурах. Ми виявили, що темепература Кюрі T_c для феромагнетика на гратці гіперкагоме (фрустрована гратка) становить приблизно $0.33|J|$, що менше за T_c для феромагнетика на гратці алмазу (інша тривимірна гратка з таким самим координаційним числом 4, але подвійна) на приблизно 25%.

Preliminaries on thermodynamics of hyperkagome-lattice $S = 1/2$ Heisenberg ferromagnet

M. Parymuda, T. Krokhmalskii, O. Derzhko

Abstract. The hyperkagome-lattice $S = 1/2$ Heisenberg ferromagnet is studied by means of (i) the linear spin-wave theory, (ii) the double-time temperature Green's functions, (iii) high-temperature expansions, and (iv) quantum Monte Carlo simulations to examine the effect of lattice geometry on the finite-temperature properties. We have found that the Curie temperature T_c for the hyperkagome-lattice (frustrated lattice) ferromagnet is about $0.33|J|$ that is smaller than T_c for the diamond-lattice (another three-dimensional lattice with the same coordination number 4 but bipartite one) ferromagnet by about 25%.

Препринти Інституту фізики конденсованих систем НАН України розповсюджуються серед наукових та інформаційних установ. Вони також доступні по електронній комп'ютерній мережі на WWW-сервері інституту за адресою http://www.icmp.lviv.ua/

The preprints of the Institute for Condensed Matter Physics of the National Academy of Sciences of Ukraine are distributed to scientific and informational institutions. They also are available by computer network from Institute's WWW server (http://www.icmp.lviv.ua/)

Максим Русланович Паримуда
Тарас Євстахійович Крохмальський
Олег Володимирович Держко

Попередні результати стосовно термодинаміки $S = 1/2$ феромагнетика Гайзенберга на гратці гіперкагоме

Роботу отримано 15 листопада 2024 р.

Затверджено до друку Вченою радою ІФКС НАН України

Рекомендовано до друку відділом квантової статистики

Виготовлено при ІФКС НАН України

1. Introduction

Frustrated quantum spin systems are a subject of intense ongoing research in the field of magnetism [1–4]. Geometric frustration and quantum fluctuations may prevent ground-state ordering even in three dimensions. Among several famous examples one may mention the $S = 1/2$ Heisenberg antiferromagnet on the kagome or pyrochlore lattices. Another interesting three-dimensional lattice is the hyperkagome lattice which has been in focus of several recent studies initiated by experiments on the spinel oxide $Na_4Ir_3O_8$ [5].

The present study concerns the $S = 1/2$ Heisenberg model on the hyperkagome lattice. However, we focus on the *ferromagnetic* sign of the exchange interaction rather than on the antiferromagnetic one. Obviously, the set of Hamiltonian eigenstates does not depend on the sign of the exchange interaction: Being arranged according to their energy, these states only invert the order under the change of the exchange interaction sign. As a result, the complicated low-energy states for the antiferromagnet must show up in the finite-temperature properties for the ferromagnet. Previously this has been illustrated for the pyrochlore lattice [6, 7]. Now, we are examining the hyperkagome lattice. 2^N eigenstates of the $S = 1/2$ ferromagnetic Heisenberg model, N is the number of lattice sites which is sent after all to infinity, lie between $-(1/2)N$ and $\approx [0.424N, 0.441N]$ [8].

There are a plenty of methods to investigate the properties of quantum Heisenberg ferromagnets. Since the ground state is "all spin up", a spin-wave theory can be elaborated straightforwardly for examining the low-temperature properties. Besides, the double-time temperature Green's function method complemented by a rotational-symmetry breaking approximation (like the Tyablikov approximation) is applicable for ferromagnets. In addition, the high-temperature expansion series for the hyperkagome-lattice $S = 1/2$ Heisenberg model are available up to 16th order [9] (see also Ref. [10]). Hence, the standard series analysis can be applied to get thermodynamic characteristics [11]. Finally, the quantum Monte Carlo method does not suffer from the infamous sign problem for ferromagnets and, for example, the ALPS package [12, 13] can be utilized for numerical study of the finite-size system thermodynamics. By comparing the outcomes of various approximate techniques we can pin down what is really inherent in the model under consideration. To some extent similar program was realized in Refs. [7, 14].

To illustrate effects of the lattice geometry, one may compare the considered model to another three-dimensional model with the same coordi-

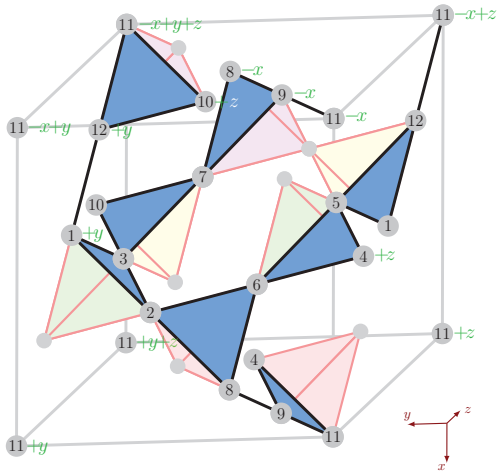

Figure 1. The hyperkagome lattice (this figure is taken from Ref. [8]). Notations are explained in the main text.

nation number 4 – the diamond-lattice $S = 1/2$ Heisenberg ferromagnet. The latter model has been discussed recently using high-temperature expansion [15, 16] and quantum Monte Carlo [17] approaches.

The paper is organized as follows. In Sections 2 and 3 we introduce the model and explain the methods to be used. Then, in Section 4, we report and discuss our main findings. Finally, we summarize in Section 5.

2. Model

2.1. Lattice

The hyperkagome lattice is a three-dimensional network of corner-sharing triangles with 12 sites in the cubic unit cell, see Fig. 1. More precisely, the sites on the hyperkagome lattice may be defined by $\boldsymbol{R}_{\boldsymbol{m}\alpha} = \boldsymbol{R}_{\boldsymbol{m}} + \boldsymbol{r}_\alpha$. Here $\boldsymbol{R}_{\boldsymbol{m}} = m_x\boldsymbol{e}_x + m_y\boldsymbol{e}_y + m_z\boldsymbol{e}_z$, where m_x, m_y, m_z are integers and $\boldsymbol{e}_x = (1,0,0)$, $\boldsymbol{e}_y = (0,1,0)$, $\boldsymbol{e}_z = (0,0,1)$. Furthermore, the origins of twelve equivalent sublattices are defined by $\boldsymbol{r}_\alpha$, $\alpha = 1, 2, \ldots, 12$, where

$$\boldsymbol{r}_1{=}\frac{1}{4}(-2,0,2),\ \boldsymbol{r}_2{=}\frac{1}{4}(-1,3,2),\ \boldsymbol{r}_3{=}\frac{1}{4}(-2,3,1),$$
$$\boldsymbol{r}_4{=}\frac{1}{4}(-1,1,0),\ \boldsymbol{r}_5{=}\frac{1}{4}(-2,1,3),\ \boldsymbol{r}_6{=}\frac{1}{4}(-1,2,3),$$

$$\boldsymbol{r}_7{=}\frac{1}{4}(-3,2,1),\ \boldsymbol{r}_8{=}\frac{1}{4}(0,2,2),\ \boldsymbol{r}_9{=}\frac{1}{4}(0,1,1),$$
$$\boldsymbol{r}_{10}{=}\frac{1}{4}(-3,3,0),\ \boldsymbol{r}_{11}{=}(0,0,0),\ \boldsymbol{r}_{12}{=}\frac{1}{4}(-3,0,3). \quad (1)$$

In Fig. 1, the site $n_x{=}n_y{=}n_z{=}0$, $\boldsymbol{r}_1$ is denoted as 1, the site $n_x{=}-1$, $n_y{=}n_z{=}1$, $\boldsymbol{r}_{11}$, i.e., $-\boldsymbol{e}_x{+}\boldsymbol{e}_y{+}\boldsymbol{e}_z{+}\boldsymbol{r}_{11}$, is denoted as $11{-}x{+}y{+}z$, and so on. Obviously, each site has 4 nearest neighbors; they are connected by a bond. Therefore, we have to consider 24 bonds: 15 bonds connecting the sites inside the unit cell, $1-5$, $1-12$, $2-3$, $2-6$, $2-8$, $3-7$, $3-10$, $4-9$, $4-11$, $5-6$, $5-12$, $6-8$, $7-10$, $8-9$, $9-11$, and 9 bonds connecting the sites from the unit cell $n_x{=}n_y{=}n_z{=}0$ to the sites from the neighboring unit cells, $1-(2{-}y)$, $1-(3{-}y)$, $4-(5{-}z)$, $4-(6{-}z)$, $7-(8{-}x)$, $7-(9{-}x)$, $10-(11{-}x{+}y)$, $10-(12{+}y{-}z)$, $11-(12{+}x{-}z)$. In Fig. 1 we show for clarity 28 bonds (thick black), i.e., besides the 15 bonds inside the unit cell, the following bonds: $(1{+}y)-2$ (equivalent to $1-(2-y)$), $(1{+}y){-}3$ (equivalent to $1-(3-y)$), $(1{+}y){-}(12{+}y)$ (cf. $1{-}12$), $(4{+}z)-5$ (equivalent to $4-(5-z)$), $(4{+}z)-6$ (equivalent to $4-(6-z)$), $7-(8{-}x)$, $7-(9{-}x)$, $(8{-}x)-(9{-}x)$ (cf. $8-9$), $(9{-}x)-(11{-}x)$ (cf. $9-11$), $(10{+}z)-(11{-}x{+}y{+}z)$ (equivalent to $10-(11{-}x{+}y)$), $(10{+}z)-(12{+}y)$ (equivalent to $10-(12{+}y{-}z)$), $(11{-}x{+}z){-}12$ (equivalent to $11-(12{+}x{-}z)$), $(11{-}x{+}y{+}z){-}12{+}y$ (cf. $11-(12{+}x{-}z)$ or $(11{-}x{+}z){-}12$).

2.2. Spin Hamiltonian

In the present study, we consider the $S = 1/2$ ferromagnetic Heisenberg model on the hyperkagome lattice given by the Hamiltonian

$$H = -|J| \sum_{\langle \boldsymbol{m}\alpha;\boldsymbol{n}\beta\rangle} \boldsymbol{S}_{\boldsymbol{m}\alpha} \cdot \boldsymbol{S}_{\boldsymbol{n}\beta}. \quad (2)$$

We may set the ferromagnetic interaction constant $|J| = 1$ this way fixing the energy scale. The sum in Eq. (2) runs over the nearest bonds of the hyperkagome lattice, which are shown in Fig. 1. The Heisenberg coupling may be also written as $\boldsymbol{S}_{\boldsymbol{m}\alpha} \cdot \boldsymbol{S}_{\boldsymbol{n}\beta} = (S^-_{\boldsymbol{m}\alpha}S^+_{\boldsymbol{n}\beta} + S^+_{\boldsymbol{m}\alpha}S^-_{\boldsymbol{n}\beta})/2 + S^z_{\boldsymbol{m}\alpha}S^z_{\boldsymbol{n}\beta}$ and $S^z = 1/2 - S^-S^+$.

For analytical calculations it is convenient to impose periodic boundary conditions and introduce the following operators

$$S^+_{\boldsymbol{q}\alpha}{=}\frac{1}{\sqrt{\mathcal{N}}}\sum_{\boldsymbol{m}} \mathrm{e}^{-\mathrm{i}\boldsymbol{q}\cdot\boldsymbol{R}_{\boldsymbol{m}}} S^+_{\boldsymbol{m}\alpha},$$
$$S^-_{\boldsymbol{q}\alpha}{=}\frac{1}{\sqrt{\mathcal{N}}}\sum_{\boldsymbol{m}} \mathrm{e}^{\mathrm{i}\boldsymbol{q}\cdot\boldsymbol{R}_{\boldsymbol{m}}} S^-_{\boldsymbol{m}\alpha}. \quad (3)$$

Here $\alpha = 1, \ldots, 12$, $\mathcal{N} = N/12$ is the number of unit cells, $\mathcal{N} = \mathcal{L}_x\mathcal{L}_y\mathcal{L}_z$, $\boldsymbol{q}\cdot\boldsymbol{R_m} = q_x m_x + q_y m_y + q_z m_z$, where $q_x = 2\pi z_x/\mathcal{L}_x$, $z_x = 1, \ldots, \mathcal{L}_x$ and so on.

3. Methods

3.1. Linear spin-wave theory

Using the Holstein-Primakoff transformation [18]

$$S^+ \approx \sqrt{2S}a, \quad S^- \approx \sqrt{2S}a^\dagger, \quad S^z = S - a^\dagger a \tag{4}$$

(in the end, we set $S = 1/2$) we get for each bond

$$\begin{aligned}\boldsymbol{S}_{\boldsymbol{m}\alpha}\cdot\boldsymbol{S}_{\boldsymbol{n}\beta}\\ \approx S^2 - S\left(a^\dagger_{\boldsymbol{m}\alpha}a_{\boldsymbol{n}\beta} + a_{\boldsymbol{m}\alpha}a^\dagger_{\boldsymbol{n}\beta} - a^\dagger_{\boldsymbol{m}\alpha}a_{\boldsymbol{m}\alpha} - a^\dagger_{\boldsymbol{n}\beta}a_{\boldsymbol{n}\beta}\right)\\ + a^\dagger_{\boldsymbol{m}\alpha}a_{\boldsymbol{m}\alpha}a^\dagger_{\boldsymbol{n}\beta}a_{\boldsymbol{n}\beta}.\end{aligned} \tag{5}$$

Note that the last term may be omitted as irrelevant for determination of the one-magnon spectrum. Next, we introduce 12 bosonic operators

$$a_{\boldsymbol{q}\alpha} = \frac{1}{\sqrt{\mathcal{N}}}\sum_{\boldsymbol{m}} \mathrm{e}^{-\mathrm{i}\boldsymbol{q}\cdot\boldsymbol{R_m}} a_{\boldsymbol{m}\alpha}, \quad \alpha = 1, \ldots, 12, \tag{6}$$

cf. Eq. (3). Furthermore, for 15 bonds connecting the sites within the same unit cell we have

$$\begin{aligned}\sum_{\boldsymbol{m}} \boldsymbol{S}_{\boldsymbol{m}\alpha}\cdot\boldsymbol{S}_{\boldsymbol{m}\beta} \to \mathcal{N}S^2\\ + S\sum_{\boldsymbol{q}}\left(a^\dagger_{\boldsymbol{q}\alpha}a_{\boldsymbol{q}\beta} + a_{\boldsymbol{q}\alpha}a^\dagger_{\boldsymbol{q}\beta} - a^\dagger_{\boldsymbol{q}\alpha}a_{\boldsymbol{q}\alpha} - a^\dagger_{\boldsymbol{q}\beta}a_{\boldsymbol{q}\beta}\right).\end{aligned} \tag{7}$$

Whereas for 9 bonds connecting the sites from neighboring unit cells, i.e., $1-(2-y)$, $1-(3-y)$, $4-(5-z)$, $4-(6-z)$, $7-(8-x)$, $7-(9-x)$, $10-(11-x+y)$, $10-(12+y-z)$, $11-(12+x-z)$ we have, for instance,

$$\begin{aligned}\sum_{\boldsymbol{m}} \boldsymbol{S}_{\boldsymbol{m}1}\cdot\boldsymbol{S}_{\boldsymbol{m}-\boldsymbol{e}_y,2} \to \mathcal{N}S^2\\ + S\sum_{\boldsymbol{q}}\left(a^\dagger_{\boldsymbol{q}1}a_{\boldsymbol{q}2}\mathrm{e}^{-\mathrm{i}q_y} + a_{\boldsymbol{q}1}a^\dagger_{\boldsymbol{q}2}\mathrm{e}^{\mathrm{i}q_y} - a^\dagger_{\boldsymbol{q}1}a_{\boldsymbol{q}1} - a^\dagger_{\boldsymbol{q}2}a_{\boldsymbol{q}2}\right),\end{aligned} \tag{8}$$

and so on. As a result, the Hamiltonian of the spin model becomes

$$\begin{aligned}H \to -24\mathcal{N}S^2|J|\\ + S|J|\sum_{\boldsymbol{q}}\begin{pmatrix} a^\dagger_{\boldsymbol{q}1} & \ldots & a^\dagger_{\boldsymbol{q}12}\end{pmatrix}\boldsymbol{F}\begin{pmatrix} a_{\boldsymbol{q}1}\\ \vdots\\ a_{\boldsymbol{q}12}\end{pmatrix},\end{aligned} \tag{9}$$

where

$$\begin{aligned} F_{\alpha\alpha} &= 4,\\ F_{12} = F_{13} &= -\mathrm{e}^{-\mathrm{i}q_y},\ F_{15} = F_{1,12} = -1,\\ F_{23} = F_{26} = F_{28} &= F_{37} = F_{3,10} = -1,\\ F_{45} = F_{46} &= -\mathrm{e}^{-\mathrm{i}q_z},\ F_{49} = F_{4,11} = -1,\\ F_{5,12} &= F_{56} = F_{68} = -1,\\ F_{78} = F_{79} &= -\mathrm{e}^{-\mathrm{i}q_x},\ F_{7,10} = F_{89} = F_{9,11} = -1,\\ F_{10,11} = -\mathrm{e}^{\mathrm{i}(q_y-q_x)}&, F_{10,12} = -\mathrm{e}^{\mathrm{i}(q_y-q_z)}, F_{10,11} = -\mathrm{e}^{\mathrm{i}(q_x-q_z)}; \end{aligned} \tag{10}$$

other matrix elements are zero and $F_{\alpha\beta} = F^*_{\beta\alpha}$. The matrix $\boldsymbol{F}$ can be brought into the diagonal form

$$\boldsymbol{U}\boldsymbol{F}\boldsymbol{U}^\dagger = \begin{pmatrix} \varepsilon_{\boldsymbol{q}1} & \ldots & 0\\ \vdots & \vdots & \vdots\\ 0 & \ldots & \varepsilon_{\boldsymbol{q}12}\end{pmatrix}. \tag{11}$$

The one-magnon energies $S|J|\varepsilon_{\boldsymbol{q}\alpha}$, $\alpha = 1, \ldots, 12$ are shown in Fig. 2.

Thermodynamic properties of noninteracting bosons with the Hamiltonian

$$H = -24\mathcal{N}S^2|J| + S|J|\sum_{\boldsymbol{q}\alpha}\varepsilon_{\boldsymbol{q}\alpha}\eta^\dagger_{\boldsymbol{q}\alpha}\eta_{\boldsymbol{q}\alpha} \tag{12}$$

can be easily calculated; they yield the low-temperature properties of the quantum spin system (2). Thus ($k_\mathrm{B} = 1$), the internal energy $E = Ne$ is given by

$$E = -24\mathcal{N}S^2|J| + S|J|\sum_{\boldsymbol{q}\alpha}\frac{\varepsilon_{\boldsymbol{q}\alpha}}{\mathrm{e}^{\frac{S|J|\varepsilon_{\boldsymbol{q}\alpha}}{T}} - 1}, \tag{13}$$

whereas the magnetization $M = Nm$ is given by

$$M = 12\mathcal{N}S - \sum_{\boldsymbol{q}\alpha}\frac{1}{\mathrm{e}^{\frac{S|J|\varepsilon_{\boldsymbol{q}\alpha}}{T}} - 1}; \tag{14}$$

here $\beta = 1/T$. As a result, the specific heat is given by $C = \partial E/\partial T$ and the entropy $S = \int_0^T \mathrm{d}TC/T$. To calculate the uniform susceptibility per site χ, we have to introduce the Zeeman term with a (small) magnetic field h ($g\mu_\mathrm{B} = 1$), calculate $\chi = \partial m/\partial h$, and then set $h = 0$. In the presence of the field, one has to replace in Eq. (12) $-24\mathcal{N}S^2|J| \to -24\mathcal{N}S^2|J| - 12\mathcal{N}Sh$ and $S|J|\varepsilon_{\boldsymbol{q}\alpha} \to S|J|\varepsilon_{\boldsymbol{q}\alpha} + h$. Thus,

$$N\chi = \frac{1}{4T}\sum_{\boldsymbol{q}\alpha}\frac{1}{\sinh^2\frac{S|J|\varepsilon_{\boldsymbol{q}\alpha}}{2T}} \tag{15}$$

(χ (15) diverges at any $T > 0$).

All above expressions can be evaluated numerically. Since for the lowest-energy (acoustic) magnon band $\varepsilon_{\boldsymbol{q}\to 0} \to \boldsymbol{q}^2/16$ (see also Fig. 2), all thermodynamic quantities show the standard behavior as $T \to 0$, i.e., $E \propto T^{5/2}$, $C \propto T^{3/2}$, $NS - M \propto T^{3/2}$, see Fig. 3 and Appendices A and B.

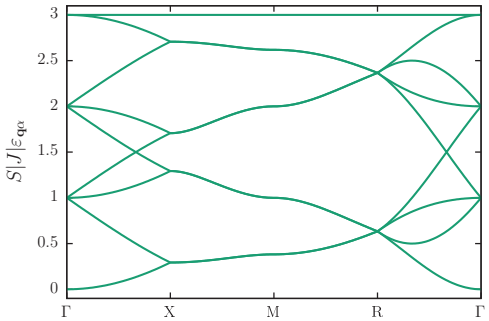

Figure 2. One-magnon bands $S|J|\varepsilon_{\boldsymbol{q}\alpha}$ along the path $\Gamma{-}X{-}M{-}R{-}\Gamma$ for the hyperkagome-lattice $S = 1/2$ Heisenberg ferromagnet. The special points in the first Brillouin zone of a simple cubic lattice are defined as follows: $\Gamma = (0,0,0)$, $X = (0,\pi,0)$, $M = (\pi,\pi,0)$, and $R = (\pi,\pi,\pi)$, see, e.g., http://lampx.tugraz.at/ hadley/ss1/bzones/sc.php . There are 12 bands in total: 8 bands are dispersive with the energy $0 \le S|J|\varepsilon_{\boldsymbol{q}\alpha} \le 3$, $\alpha = 1,\ldots,8$ and 4 bands are dispersionless (flat) with the energy $S|J|\varepsilon_{\boldsymbol{q}\alpha} = 3$, $\alpha = 9,\ldots,12$.

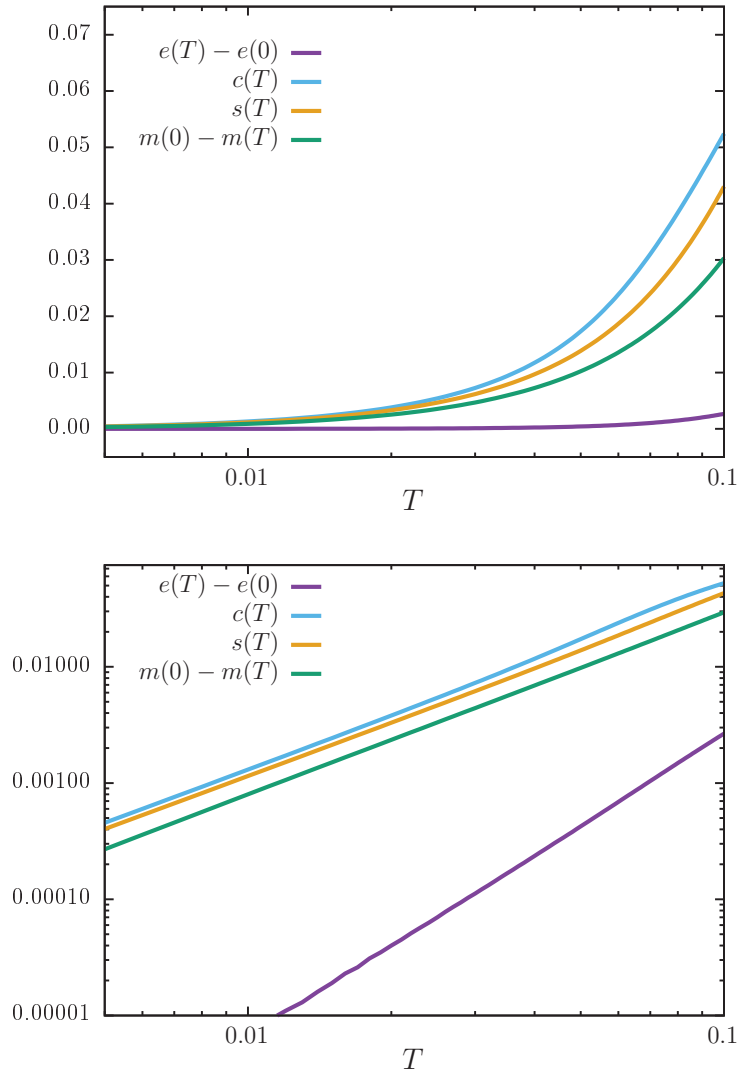

Figure 3. Linear spin-wave theory for the low-temperature thermodynamics. We show temperature dependencies of $e - e_0$, c, s, and $S - m$ in (top) semilogarithmic scale as well as in (bottom) double logarithmic scale to illustrate the power-law exponents as $T \to 0$.

3.2. Green's function method: Mean-field and random-phase approximations

We introduce the (retarded) Green's functions ($\hbar = 1$) [19]

$$G_{\alpha\beta}(t) \equiv \langle\langle S^+_{\boldsymbol{q}\alpha} | S^-_{\boldsymbol{q}\beta}\rangle\rangle_t = -\mathrm{i}\Theta(t)\langle[S^+_{\boldsymbol{q}\alpha}(t), S^-_{\boldsymbol{q}\beta}]\rangle,$$

$$G_{\alpha\beta} \equiv G_{\alpha\beta}(\omega) = \int\limits_{-\infty}^{\infty} \mathrm{d}t \mathrm{e}^{\mathrm{i}\omega t} G_{\alpha\beta}(t), \tag{16}$$

where the operators $S^{\pm}_{\boldsymbol{q}\alpha}$ are defined in Eq. (3). $G_{\alpha\beta}(\omega)$ gives immediately the dynamic susceptibility $\chi^{+-}_{\boldsymbol{q}}(\omega) = -\sum_{\alpha,\beta=1}^{12} G_{\alpha\beta}(\omega)/12$ and the correlation functions $\langle S^-_{\boldsymbol{q}\beta}(t) S^+_{\boldsymbol{q}\alpha}\rangle = [\mathrm{i}/(2\pi)] \lim_{\epsilon\to 0} \int_{-\infty}^{\infty} \mathrm{d}\omega \mathrm{e}^{-\mathrm{i}\omega t} [G_{\alpha\beta}(\omega + \mathrm{i}\epsilon) - G_{\alpha\beta}(\omega - \mathrm{i}\epsilon)]/(\mathrm{e}^{\omega/T} - 1)$. Equal-time correlations yield thermodynamics. In particular, the magnetization per site $m = \langle S^z\rangle$ is given by $\langle S^z\rangle = 1/2 - (1/N)\sum_{\boldsymbol{q}\alpha}\langle S^-_{\boldsymbol{q}\alpha} S^+_{\boldsymbol{q}\alpha}\rangle$. To calculate the Green's function, we use the equation of motion method [19].

To begin, we consider the simplest mean-field version of the Hamiltonian (2)

$$H = 2N|J|\langle S^z\rangle^2 - 4|J|\langle S^z\rangle \sum_{\boldsymbol{m}}\sum_{\alpha} S^z_{\boldsymbol{m}\alpha}. \tag{17}$$

The exact first-order equation of motion gives

$$G_{\alpha\beta} = \frac{2\langle S^z\rangle\delta_{\alpha\beta}}{\omega - 4|J|\langle S^z\rangle}, \quad \langle S^-_{\boldsymbol{q}\beta} S^+_{\boldsymbol{q}\alpha}\rangle = \frac{2\langle S^z\rangle\delta_{\alpha\beta}}{\mathrm{e}^{\frac{4|J|\langle S^z\rangle}{T}} - 1}, \tag{18}$$

and, as a result, $\langle S^z\rangle$ satisfies the self-consistent equation

$$1 = 2\langle S^z\rangle \coth\frac{2|J|\langle S^z\rangle}{T} \tag{19}$$

This equation yields the mean-field prediction for the Curie temperature $T_c/|J| = 1$, which depends only on the number of the nearest neighbors, with $\langle S^z\rangle \le 1/2$ for $T < T_c$ but $\langle S^z\rangle = 0$ for $T \ge T_c$. In Fig. 4 we illustrate the solution of this equation. Thermodynamics within the mean-field approximation can be obtained from the internal energy $E = -2N|J|\langle S^z\rangle^2$.

Next, we do not break explicitly the rotational-invariant symmetry of the spin Hamiltonian (2), but write down the first-order equation of motion, and calculate the following time derivative

$$\dot{S}^+_{\boldsymbol{q}\alpha} = \frac{\mathrm{i}}{\sqrt{\mathcal{N}}} \sum_{\boldsymbol{m}} \mathrm{e}^{-\mathrm{i}\boldsymbol{q}\cdot\boldsymbol{R}_{\boldsymbol{m}}} \left[H, S^+_{\boldsymbol{m}\alpha}\right]. \tag{20}$$

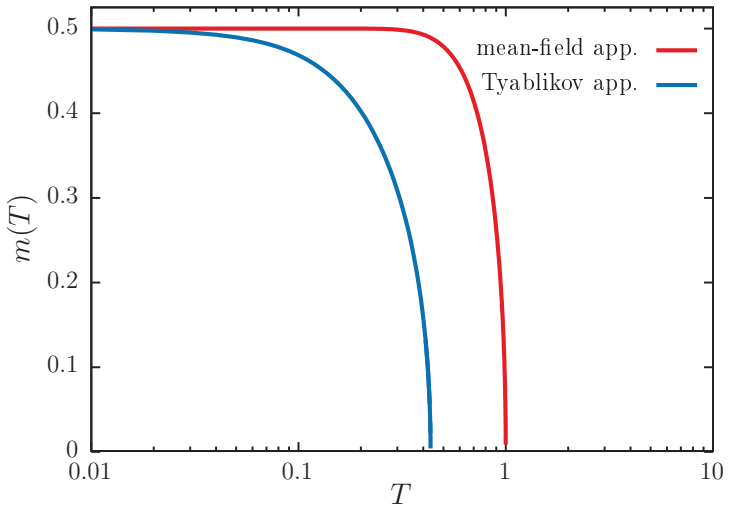

Figure 4. Magnetization of the hyperkagome-lattice $S = 1/2$ Heisenberg ferromagnet as it follows from Eq. (19) (mean-field approximation) and Eq. (24) (Tyablikov approximation).

Note that each site has only 4 neighboring sites. Furthermore,

$$[\boldsymbol{S}_A\cdot\boldsymbol{S}_B, S^+_B] = -S^+_A S^z_B + S^z_A S^+_B \to \langle S^z\rangle\left(-S^+_A + S^+_B\right)$$

(Tyablikov approximation). As a result, we have, e.g.,

$$\omega G_{1\beta} = 2\langle S^z\rangle\delta_{1\beta}$$
$$+|J|\langle S^z\rangle\left(4G_{1\beta} - \mathrm{e}^{-\mathrm{i}q_y} G_{2\beta} - \mathrm{e}^{-\mathrm{i}q_y} G_{3\beta} - G_{5\beta} - G_{12,\beta}\right) \tag{21}$$

and so on or in the matrix form

$$(\omega\mathbf{1} - |J|\langle S^z\rangle\boldsymbol{F})\ \boldsymbol{G} = 2\langle S^z\rangle\mathbf{1}, \tag{22}$$

where the matrix $\boldsymbol{F}$ is defined in Eq. (10). Knowing the eigenvectors $\langle\beta|\boldsymbol{q}\gamma\rangle$, $\beta = 1, \ldots, 12$ and the corresponding eigenvalues $\varepsilon_{\boldsymbol{q}\gamma}$ of the matrix $\boldsymbol{F}$, i.e., $\sum_\beta F_{\alpha\beta}\langle\beta|\boldsymbol{q}\gamma\rangle = \varepsilon_{\boldsymbol{q}\gamma}\langle\alpha|\boldsymbol{q}\gamma\rangle$, we can get the desired result

$$G_{\alpha\beta} = 2\langle S^z\rangle \sum_{\gamma=1}^{12} \frac{\langle\alpha|\boldsymbol{q}\gamma\rangle\langle\boldsymbol{q}\gamma|\beta\rangle}{\omega - |J|\langle S^z\rangle\varepsilon_{\boldsymbol{q}\gamma}}. \tag{23}$$

The eigenvectors $\langle\alpha|\boldsymbol{q}\gamma\rangle$ and $\langle\boldsymbol{q}\gamma|\beta\rangle$ appearing in Eq. (23) are not explicitly calculated, since $\langle S^z\rangle$ contains after all $\sum_\alpha\langle\alpha|\boldsymbol{q}\gamma\rangle\langle\boldsymbol{q}\gamma|\alpha\rangle = 1$. Therefore, we arrive at the following equation for $\langle S^z\rangle$:

$$\langle S^z\rangle = \frac{1}{2} - \frac{\langle S^z\rangle}{6\mathcal{N}} \sum_{\gamma=1}^{12} \sum_{\boldsymbol{q}} \frac{1}{\mathrm{e}^{\frac{|J|\langle S^z\rangle\varepsilon_{\boldsymbol{q}\gamma}}{T}} - 1}. \tag{24}$$

In Fig. 4 we illustrate the solution of this equation.

Equation for $\langle S^z\rangle$ (24) at T_c, where $\langle S^z\rangle$ vanishes, yields the following Curie temperature T_c:

$$\frac{T_c}{|J|} = \frac{3}{\sum_\gamma \frac{1}{\mathcal{N}} \sum_{\boldsymbol{q}} \frac{1}{\varepsilon_{\boldsymbol{q}\gamma}}} \approx 0.433\,8. \tag{25}$$

Here, we have used that in the thermodynamic limit $\sum_{\boldsymbol{q}}(\ldots)/\mathcal{N}$ becomes $\int_{-\pi}^{\pi}\mathrm{d}q_x\int_{-\pi}^{\pi}\mathrm{d}q_y\int_{-\pi}^{\pi}\mathrm{d}q_z(\ldots)/(8\pi^3)$.

Further analysis of thermodynamics within the Tyablikov approximation can be performed as in Ref. [7], where the pyrochlore-lattice case was examined.

3.3. High-temperature expansion series and the Curie temperature

Using the high-temperature expansion series with respect to $\beta = 1/T$ reported in Ref. [9], that is,

$$\frac{\chi(\beta)}{\beta} = \sum_{n=0}^{16} \frac{b_n}{4^n}\beta^n \tag{26}$$

with the series expansion coefficients b_n given in Table I of Ref. [9], we can find the Curie temperature $T_c = 1/\beta_c$, see, e.g., Ref. [11]. Really, since $\chi \propto (\beta_c - \beta)^{-\gamma}$ for $\beta \approx \beta_c$, $\beta < \beta_c$ ($\gamma > 0$ is a critial exponent), one has $\chi(\beta)/\chi'(\beta) = (\beta_c - \beta)/\gamma$. Now a ratio of two polynomials $\chi(\beta)$ and $\chi'(\beta)$ obtained according to Eq. (26) is re-expanded in powers of β. For the resulting polynomial of order 16 we construct a number of Padé approximants $[u, d]$ to this result, $u + d \le 16$, and seek for each of them the least positive root, β_c and the slope at β_c.

The so obtained approximate values of $T_c = 1/\beta_c$ are collected in Table 1. The arithmetic mean of 15 values of T_c reported in Table 1 gives $T_c \approx 0.326$. If we drop out two largest deviations from the mean value and then find the arithmetic mean of 13 values of T_c we get $T_c \approx 0.338\pm0.044$. For γ we get the arithmetic mean $\gamma \approx 1.87$ or, after omitting two largest deviations from the mean value, $\gamma \approx 1.44$.

Table 1. Estimates of T_c and γ (in brackets) from $[u, d]$ Padé approximants to the series $\chi(\beta)/\chi'(\beta)$.

	$u=6$	$u=7$	$u=8$
$d=4$	0.351 (1.191)	0.354 (1.163)	0.331 (1.554)
$d=5$	0.354 (1.162)	0.351 (1.189)	0.361 (1.113)
$d=6$	0.336 (1.417)	0.363 (1.096)	0.348 (1.211)
$d=7$	0.262 (4.101)	0.295 (2.376)	0.329 (1.449)
$d=8$	0.323 (1.389)	0.245 (5.268)	0.294 (2.406)

3.4. Quantum Monte Carlo simulations

In our study, we also use the ALPS package (directed-loop scheme in SSE method) [12, 13] to perform quantum Monte Carlo simulations. We consider periodic lattices of $\mathcal{N} = \mathcal{L}^3$ unit cells with $\mathcal{L} = 1, 2, 3, 4, 5, 10, 20$, 30, and 40. In our simulations, we introduce a small (symmetry-breaking) magnetic field along z direction with $h = 10^{-4}$, 10^{-5}, or 10^{-6}. From the ALPS package computations we obtain temperature dependencies of the internal energy E, the magnetization $\langle\sum_j S_j^z\rangle$, and $\langle(\sum_j S_j^z)^2\rangle$. Then we calculate the specific heat, the entropy, and the susceptibility:

$$C = \frac{\partial E}{\partial T},$$
$$S = \int_0^T \mathrm{d}T\frac{C(T)}{T} = N\ln 2 - \int_T^\infty \mathrm{d}T\frac{C(T)}{T},$$
$$N\chi = \frac{\langle(\sum_j S_j^z)^2\rangle - \langle\sum_j S_j^z\rangle^2}{T}. \tag{27}$$

The results for $\mathcal{N} = 1$ obtained by exact diagonalization and quantum Monte Carlo simulations are in a perfect agreement, see Figs. 5 and 6. An interplay of the value of h and system size $\mathcal{N}$ for determining of the temperature dependence of magnetization is illustrated in Fig. 7.

Finite-size data may be plugged into an ansatz which appears after differentiating the free energy [20]

$$F_{\mathcal{L}} = \mathcal{L}^\gamma f\left(t\mathcal{L}^{\frac{1}{\nu}}, h\mathcal{L}^{\frac{\beta\delta}{\nu}}\right), \quad t \equiv \left|1 - \frac{T}{T_c}\right|. \tag{28}$$

Another way around is to call $T_c(\mathcal{L})$ the temperature associated with the maximum of the finite thermodynamic quantities, namely the “effective

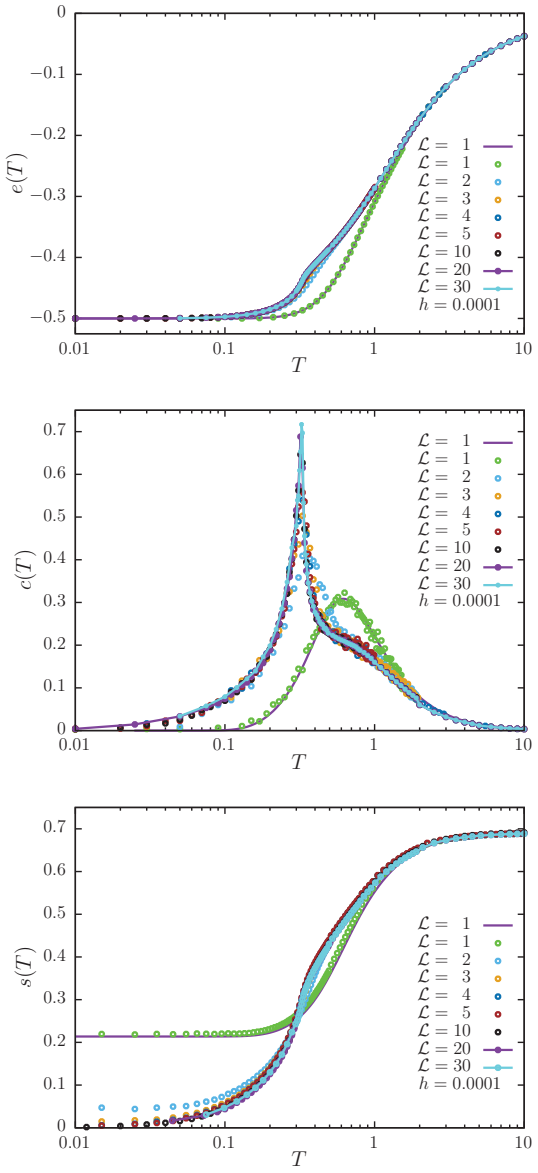

Figure 5. Thermodynamics of the hyperkagome-lattice $S = 1/2$ Heisenberg ferromagnet. Quantum Monte Carlo simulations for (from top to bottom) internal energy, specific heat, and entropy. The value of the symmetry-breaking field is $h = 10^{-4}$.

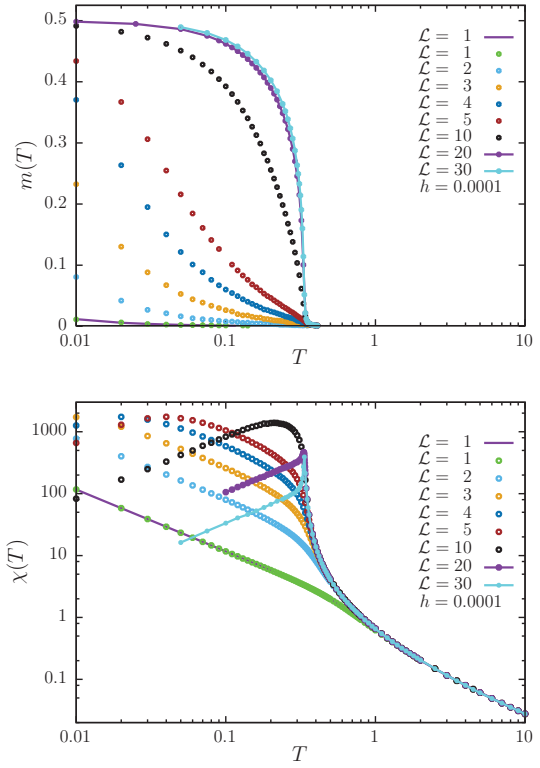

Figure 6. Thermodynamics of the hyperkagome-lattice $S = 1/2$ Heisenberg ferromagnet. Quantum Monte Carlo simulations for (from top to bottom) magnetization and susceptibility. The value of the symmetry-breaking field is $h = 10^{-4}$.

critical temperature". It varies as follows (Ref. [21], page 3): $T_c - T_c(\mathcal{L}) \sim \mathcal{L}^{-1/\nu}$. By studying $T_c(\mathcal{L})$ for different $\mathcal{L}$, one can extract T_c and ν.

4. Results and discussion

Let us discuss the thermodynamic quantities for the hyperkagome-lattice $S = 1/2$ Heisenberg antiferromagnet as they are predicted by different methods, see Fig. 8 and Table 2. Conventional linear spin-wave theory gives the standard power-law decay exponents for the internal en-

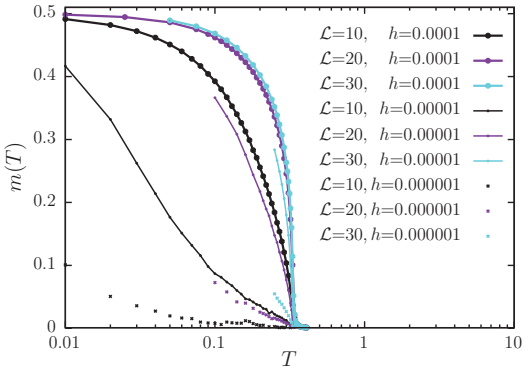

Figure 7. Quantum Monte Carlo simulations for the magnetization of the hyperkagome-lattice $S = 1/2$ Heisenberg ferromagnet. The values of the symmetry-breaking field are $h = 10^{-4}$, 10^{-5}, and 10^{-6}.

Table 2. The Curie temperature T_c as it follows from different approaches.

mean-field approximation	1
Tyablikov approximation	0.434
high-temperature expansion series	0.338 ± 0.044
quantum Monte Carlo simulations	0.330 ± 0.004

ergy and magnetization as $T \to 0$; the prefactors are related to the lattice geometry, which determines the coefficient for the (quadratic) spin-wave decay in the Γ point, see Fig. 2. The double-time temperature Green's function method within the mean-field and Tyablikov approximations yields qualitatively correct results not only at low temperatures, but also at intermediate temperatures. It predicts a reasonable temperature dependence of the magnetization in the ordered phase and the value of the Curie temperature: $T_c/|J| = 1$ (mean-field approximation) and $T_c/|J| \approx 0.434$ (Tyablikov approximation), see Table 2. These results underestimate temperature fluctuations and the true Curie temperature is lower. Thus, high-temperature expansion series for the uniform susceptibility $\chi(\beta)$ up to β^{16} [9] leads to a lower value of T_c: $T_c/|J| \approx 0.338 \pm 0.044$, whereas quantum Monte Carlo simulations

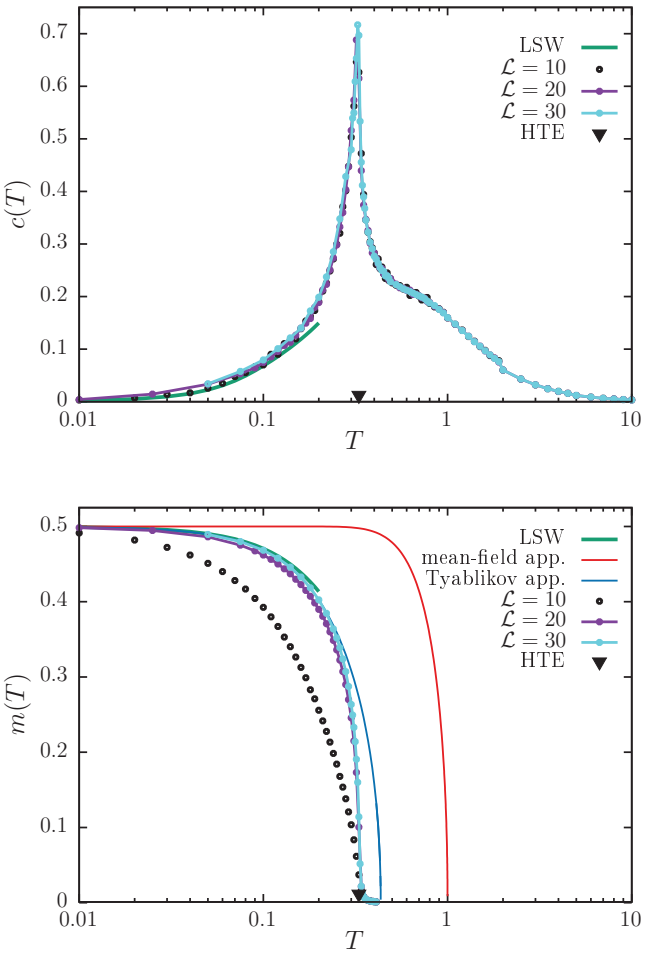

Figure 8. Thermodynamics of the hyperkagome-lattice $S = 1/2$ Heisenberg ferromagnet: Temperature dependence of (top) specific heat and (bottom) magnetization. We report linear spin-wave results, Green's function calculations (mean-field and Tyablikov approximations), quantum Monte Carlo simulations for large enough systems with the symmetry-breaking field is $h = 0.000\,1$, and high-temperature expansion series analysis for T_c.

suggest $T_c/|J| \approx 0.330 \pm 0.004$ (according to the magnetization and the susceptibility (Fig. 6)). High-temperature expansion series are valid not only in the disorder phase, but also can be used to determine the critical behavior around the Curie temperature. In particular, the obtained approximately γ exponent, $\gamma \approx 1.44$, indicates that the model at hand belongs to the three-dimensional Heisenberg universality class with the critical exponents $\gamma = 1.396\,0(9)$, $\nu = 0.711\,2(5)$, $\eta = 0.037\,5(5)$, $\alpha = -0.133\,6(15)$, $\beta = 0.368\,9(3)$, and $\delta = 4.783(3)$ [22]. Critical exponents for the three-dimensional Heisenberg universality class rounded to two decimal places according to Ref. [23] are as follows: $\alpha = -0.12$, $\beta = 0.36$, $\gamma = 1.39$, $\delta = 4.91$ $\eta = 0.04$, and $\nu = 0.71$. Finally, the most informative findings come from the quantum Monte Carlo simulations for the system size up to $N = 768\,000$ sites ($\mathcal{N} = 64\,000$ unit cells): Temperature dependence for various thermodynamic quantities refer to the whole temperature range, including the low-temperature ordered phase, the critical region around T_c, and the high-temperature disordered phase. Note that $c(T)$ exhibits a shoulder above T_c, see Figs. 5 and 8.

As has been mentioned in Sec. 1, a model with the *ferromagnetic* sign of exchange interaction at finite temperatures has some indication of its antiferromagnetic counterpart at low temperatures. In particular, intricate low-temperature states of frustrated quantum spin system should show up at finite temperatures as the sign of exchange interaction changes. To illustrate such a correspondence, we may compare the $S = 1/2$ Heisenberg model on two three-dimensional lattices both with coordination number 4: The hyperkagome lattice and the diamond lattice. Antiferromagnetic Heisenberg exchange interaction for the former lattice is frustrated, whereas the latter bipartite lattice supports the Néel order. Now, the Curie temperature T_c for the diamond-lattice $S = 1/2$ Heisenberg ferromagnet is 0.447 ± 0.001 (high-temperature expansion) [15], ≈ 0.445 (high-temperature expansion) [16], or $0.444\,47(5)$ (quantum Monte Carlo simulations) [17], i.e., $T_c \approx 0.44$ is substantially higher than $T_c \approx 0.33$ for the hyperkagome-lattice case.

Finally, with our study, we have illustrated that the larger coordination number is, the better agreement with mean-field approach: The mean-field T_c for the simple-cubic and pyrochlore lattices (coordination number is 6) is 3/2 that exceeds the quantum Monte Carlo results by 79% and 109%, respectively. Now, the mean-field T_c for the diamond and hyperkagome lattices (coordination number is 4) is 1 that exceeds the quantum Monte Carlo results by about 125% and 200%, respectively.

5. Summary

To study thermodynamics of the hyperkagome-lattice $S = 1/2$ Heisenberg ferromagnet we have used four complimentary approaches: The linear spin-wave theory, which gives thermodynamics for thermodynamically large systems at low temperatures, the Green's function method augmented by the mean-field or Tyablikov approximation, which gives approximate thermodynamics for thermodynamically large systems up to the Curie temperature, high-temperature expansion series, which yield results for thermodynamically large systems but only at high and intermediate temperatures, and quantum Monte Carlo simulations, which work for all temperatures but are always performed for finite systems (in our study, up to $\mathcal{N} = 40^3$ unit cells). In general, the studied quantum Heisenberg ferromagnet exhibits the properties which are qualitatively similar to such properties of other three-dimensional quantum Heisenberg ferromagnets (power-law exponents for thermodynamic quantities as $T \to 0$, a finite Curie temperature T_c, the critical behavior of the three-dimensional Heisenberg universality class around T_c, or paramagnetic behavior as $T \to \infty$). However, the peculiarity of the hyperkagome lattice (low coordination number, geometrical frustration, i.e., conflicting antiferromagnetic interactions) leads to some quantitative differences, e.g., the value of T_c is rather small: $T_c \approx 0.33|J|$.

Let us briefly mention what is beyond our study. The simple linear spin-wave theory might be replaced by a nonlinear spin-wave theory, see, e.g., Refs. [24, 25]. The Green's function method might be augmented by more sophisticated Kondo-Yamaji approximation [26–28] which allows to study not only the ordered (ferromagnetic) region, but also the disordered (paramagnetic) region. Owing to the recent paper [10] it seems possible to obtain more coefficients in the r.h.s. of Eq. (26) and, as a result, more accurate estimates for T_c and γ (and also for other quantities) are reachable. Finally, quantum Monte Carlo simulation data could be plugged into a machinery of the finite-size scaling theory to get precise numerical values for the quantities of interest in the thermodynamic limit. Investigations along such directions may become useful if corresponding solid-state compounds come into being.

Acknowledgements

The authors are thankful to the Armed Forces of Ukraine for protection since 2014, and especially since February 24, 2022. This project is funded by the National Research Foundation of Ukraine (2023.03/0063,

Frustrated quantum magnets under various external conditions). The authors thank Taras Hutak, Taras Verkholyak, and Petro Sapriianchuk for discussions and useful comments. O. D. is grateful to Joachim Stolze and Götz Uhrig for hospitality at TU Dortmund University in November 2023.

Appendix A: Some details about linear spin-wave theory calculations for the hyperkagome-lattice case

Within the framework of the linear spin-wave theory we have to do the following integral (see Eq. (13)):

$$\begin{aligned}\frac{1}{12\mathcal{N}}\sum_{\boldsymbol{q}\alpha}\frac{S|J|\varepsilon_{\boldsymbol{q}\alpha}}{\mathrm{e}^{\frac{S|J|\varepsilon_{\boldsymbol{q}\alpha}}{T}}-1}&=\frac{1}{12(2\pi)^3}\int\mathrm{d}\boldsymbol{q}\frac{S|J|\varepsilon_{\boldsymbol{q}\alpha}}{\mathrm{e}^{\frac{S|J|\varepsilon_{\boldsymbol{q}\alpha}}{T}}-1}\\&=\frac{4\pi}{12(2\pi)^3}\int\limits_0^\infty\mathrm{d}qq^2\frac{S|J|\varepsilon_{\boldsymbol{q}\alpha}}{\mathrm{e}^{\frac{S|J|\varepsilon_{\boldsymbol{q}\alpha}}{T}}-1}=\left|S|J|\varepsilon_{\boldsymbol{q}\alpha}=\omega q^2\right|\\&=\frac{1}{24\pi^2}\int\limits_0^\infty\mathrm{d}qq^2\frac{\omega q^2}{\mathrm{e}^{\frac{\omega q^2}{T}}-1}=\left|\frac{\omega q^2}{T}=x\right|\\&=\frac{1}{48\pi^2}\frac{T^{\frac{5}{2}}}{\omega^{\frac{3}{2}}}\int\limits_0^\infty\mathrm{d}x\frac{x^{\frac{3}{2}}}{\mathrm{e}^x-1}=\frac{1}{48\pi^2\omega^{\frac{3}{2}}}\Gamma\left(\frac{5}{2}\right)\zeta\left(\frac{5}{2}\right)T^{\frac{5}{2}}\\&=\left|\omega=\frac{1}{32}\right|=\left(\frac{2}{\pi}\right)^{\frac{3}{2}}\zeta\left(\frac{5}{2}\right)T^{\frac{5}{2}}\approx 0.681\,404T^{\frac{5}{2}}.\end{aligned}\tag{A1}$$

As a result, we get in the low-temperature limit the following formulae:

$$e\approx-\frac{1}{2}+\left(\frac{2}{\pi}\right)^{\frac{3}{2}}\zeta\left(\frac{5}{2}\right)T^{\frac{5}{2}}\approx-\frac{1}{2}+0.681\,404T^{\frac{5}{2}},\tag{A2}$$

$$c\approx\frac{5}{2}\left(\frac{2}{\pi}\right)^{\frac{3}{2}}\zeta\left(\frac{5}{2}\right)T^{\frac{3}{2}}\approx 1.703\,51T^{\frac{3}{2}},\tag{A3}$$

and

$$s\approx\frac{5}{3}\left(\frac{2}{\pi}\right)^{\frac{3}{2}}\zeta\left(\frac{5}{2}\right)T^{\frac{3}{2}}\approx 1.135\,67T^{\frac{3}{2}}.\tag{A4}$$

Obviously,

$$c\approx aT^\mu,\quad s\approx\frac{c}{\mu}.\tag{A5}$$

And finally

$$m\approx\frac{1}{2}-\frac{2}{3}\left(\frac{2}{\pi}\right)^{\frac{3}{2}}\zeta\left(\frac{3}{2}\right)T^{\frac{3}{2}}\approx\frac{1}{2}-0.884\,61T^{\frac{3}{2}}.\tag{A6}$$

Appendix B: Simple-cubic-lattice case

As a reference for the hyperkagome-lattice case, although with the coordination number 6, we may consider the simple-cubic-lattice case. For the simple cubic lattice, a linear spin-wave theory deals with the Hamiltonian ($S=1/2$)

$$\begin{aligned}H\to-S|J|\sum_{\boldsymbol{q}}\big(&a^\dagger_{\boldsymbol{q}}a_{\boldsymbol{q}}\mathrm{e}^{-\mathrm{i}q_x}+a^\dagger_{\boldsymbol{q}}a_{\boldsymbol{q}}\mathrm{e}^{\mathrm{i}q_x}-2a^\dagger_{\boldsymbol{q}}a_{\boldsymbol{q}}+S\\&+a^\dagger_{\boldsymbol{q}}a_{\boldsymbol{q}}\mathrm{e}^{-\mathrm{i}q_y}+a^\dagger_{\boldsymbol{q}}a_{\boldsymbol{q}}\mathrm{e}^{\mathrm{i}q_y}-2a^\dagger_{\boldsymbol{q}}a_{\boldsymbol{q}}+S\\&a^\dagger_{\boldsymbol{q}}a_{\boldsymbol{q}}\mathrm{e}^{-\mathrm{i}q_z}+a^\dagger_{\boldsymbol{q}}a_{\boldsymbol{q}}\mathrm{e}^{\mathrm{i}q_z}-2a^\dagger_{\boldsymbol{q}}a_{\boldsymbol{q}}+S\big)\\&=-3\mathcal{N}S^2|J|+S|J|\sum_{\boldsymbol{q}}\varepsilon_{\boldsymbol{q}}a^\dagger_{\boldsymbol{q}}a_{\boldsymbol{q}},\\S|J|\varepsilon_{\boldsymbol{q}}&=2S|J|\,(3-\cos q_x-\cos q_y-\cos q_z)\\&\to S|J|\boldsymbol{q}^2.\end{aligned}\tag{B1}$$

Now the internal energy

$$E=-3\mathcal{N}S^2|J|+S|J|\sum_{\boldsymbol{q}}\frac{\varepsilon_{\boldsymbol{q}}}{\mathrm{e}^{\frac{S|J|\varepsilon_{\boldsymbol{q}}}{T}}-1}\tag{B2}$$

and the magnetization

$$M=\mathcal{N}S-\sum_{\boldsymbol{q}}\frac{1}{\mathrm{e}^{\frac{S|J|\varepsilon_{\boldsymbol{q}}}{T}}-1},\tag{B3}$$

cf. Eqs. (13) and (14). In the thermodynamic limit

$$\sum_{\boldsymbol{q}}(\ldots)/\mathcal{N}\to\int_0^\infty\mathrm{d}qq^2(\ldots)/(2\pi^2).$$

In the low-temperature limit,

$$\frac{E}{\mathcal{N}} = -\frac{3}{4}|J| + \frac{4\pi}{8\pi^3}\int\limits_0^\infty \mathrm{d}q q^2 \frac{\frac{|J|q^2}{2}}{\mathrm{e}^{\frac{|J|q^2}{2T}}-1} \tag{B4}$$

and

$$\frac{E}{\mathcal{N}|J|} = -\frac{3}{4} + \frac{\tau^{\frac{5}{2}}}{\sqrt{2}\pi^2}\int\limits_0^\infty \mathrm{d}x \frac{x^{\frac{3}{2}}}{\mathrm{e}^x-1}, \quad \tau = \frac{T}{|J|}. \tag{B5}$$

We have set already $S = 1/2$. Since

$$\begin{gathered}\int\limits_0^\infty \mathrm{d}x \frac{x^{\alpha-1}}{\mathrm{e}^x-1} = \Gamma(\alpha)\zeta(\alpha),\\ \Gamma\left(\frac{1}{2}\right)=\sqrt{\pi}, \quad \Gamma\left(\frac{3}{2}\right)=\frac{\sqrt{\pi}}{2}, \quad \Gamma\left(\frac{5}{2}\right)=\frac{3\sqrt{\pi}}{4},\\ \zeta\left(\frac{3}{2}\right)=2.612\,3\ldots, \quad \zeta\left(\frac{5}{2}\right)=1.341\,48\ldots,\end{gathered} \tag{B6}$$

we get

$$\frac{e}{|J|} + \frac{3}{4} \approx 0.128\tau^{\frac{5}{2}}. \tag{B7}$$

Then we immediately obtain the specific heat c and the entropy s.

Concerning the magnetization, we have

$$\begin{aligned}\frac{M}{\mathcal{N}} &= \frac{1}{2} - \frac{1}{\mathcal{N}}\sum_{\boldsymbol{q}} \frac{1}{\mathrm{e}^{\frac{\varepsilon_{\boldsymbol{q}}}{T}}-1}\\ &\to \frac{1}{2} - \frac{\tau^{\frac{3}{2}}}{\sqrt{2}\pi^2}\int\limits_0^\infty \mathrm{d}x \frac{x^{\frac{1}{2}}}{\mathrm{e}^x-1}\\ &= \frac{1}{2} - \frac{\tau^{\frac{3}{2}}}{\sqrt{2}\pi^2}\Gamma\left(\frac{3}{2}\right)\zeta\left(\frac{3}{2}\right)\end{aligned} \tag{B8}$$

and therefore

$$\frac{1}{2} - m \approx 0.166\tau^{\frac{3}{2}}. \tag{B9}$$

It can be noted that the prefactors in the power-law decay of thermodynamic functions for the simple-cubic case differs from the ones for the hyperkagome case; this can be traced to the difference in decay of the acoustic excitations: $\varepsilon_{\boldsymbol{q}\to 0} \to \boldsymbol{q}^2$ (simple-cubic) versus $\varepsilon_{\boldsymbol{q}\to 0} \to \boldsymbol{q}^2/16$ (hyperkagome).

We also recall here the results of the Green's function method: $T_c = 3/2$ (mean-field approximation), $T_c \approx 0.989$ (Tyablikov approximation), $T_c \approx 0.926$ (Kondo-Yamaji approximation), see Ref. [28]. Furthermore, high-temperature expansion series yields $T_c \approx 0.838\,9$ [16], whereas quantum Monte Carlo simulations result in $T_c \approx 0.839(1)$ [29].

References

1. C. Berthier, L. P. Lévy, and G. Martinez, eds., *High Magnetic Fields: Applications in Condensed Matter Physics and Spectroscopy*, Vol. 595 (Springer Berlin, Heidelberg, 2002).
2. U. Schollwöck, J. Richter, D. J. J. Farnell, and R. F. Bishop, eds., *Quantum Magnetism*, Vol. 645 (Springer Berlin, Heidelberg, 2004).
3. H. T. Diep, ed., *Frustrated Spin Systems* (World Scientific, Singapore, 2005).
4. C. Lacroix, P. Mendels, and F. Mila, *Introduction to Frustrated Magnetism: Materials, Experiments, Theory*, Springer Series in Solid-State Sciences (Springer Berlin Heidelberg, 2011).
5. Y. Okamoto, M. Nohara, H. Aruga-Katori, and H. Takagi, Phys. Rev. Lett. **99**, 137207 (2007).
6. P. Müller, A. Lohmann, J. Richter, O. Menchyshyn, and O. Derzhko, Phys. Rev. B **96**, 174419 (2017).
7. T. Hutak, P. Müller, J. Richter, T. Krokhmalskii, and O. Derzhko, Condensed Matter Physics **21**, 33705 (2018).
8. T. Hutak, T. Krokhmalskii, J. Schnack, J. Richter, and O. Derzhko, Phys. Rev. B **110**, 054428 (2024).
9. R. R. P. Singh and J. Oitmaa, Phys. Rev. B **85**, 104406 (2012).
10. L. Pierre, B. Bernu, and L. Messio, SciPost Phys. **17**, 105 (2024).
11. J. Oitmaa, C. Hamer, and W. Zheng, *Series Expansion Methods for Strongly Interacting Lattice Models* (Cambridge University Press, 2006).
12. A. Albuquerque, F. Alet, P. Corboz, P. Dayal, A. Feiguin, S. Fuchs, L. Gamper, E. Gull, S. Gürtler, A. Honecker, R. Igarashi, M. Körner, A. Kozhevnikov, A. Läuchli, S. Manmana, M. Matsumoto, I. McCulloch, F. Michel, R. Noack, G. Pawłowski, L. Pollet, T. Pruschke, U. Schollwöck, S. Todo, S. Trebst, M. Troyer, P. Werner, and S. Wessel, Journal of Magnetism and Magnetic Materials **310**, 1187 (2007), Proceedings of the 17th International Conference on Magnetism.

13. B. Bauer, L. D. Carr, H. G. Evertz, A. Feiguin, J. Freire, S. Fuchs, L. Gamper, J. Gukelberger, E. Gull, S. Guertler, A. Hehn, R. Igarashi, S. V. Isakov, D. Koop, P. N. Ma, P. Mates, H. Matsuo, O. Parcollet, G. Pawłowski, J. D. Picon, L. Pollet, E. Santos, V. W. Scarola, U. Schollwöck, C. Silva, B. Surer, S. Todo, S. Trebst, M. Troyer, M. L. Wall, P. Werner, and S. Wessel, Journal of Statistical Mechanics: Theory and Experiment **2011**, P05001 (2011).
14. V. R. Pavizhakumari, T. Skovhus, and T. Olsen, Beyond the random phase approximation for calculating Curie temperatures in ferromagnets: application to Fe, Ni, Co and monolayer CrI_3 (2024), arXiv:2405.00477 [cond-mat.mtrl-sci] .
15. J. Oitmaa, Journal of Physics: Condensed Matter **30**, 155801 (2018).
16. M. D. Kuz'min, Philosophical Magazine Letters **99**, 338 (2019).
17. R. Bärwolf, A. Sushchyev, F. P. Toldin, and S. Wessel, Phase transitions in the spin-1/2 Heisenberg antiferromagnet on the dimerized diamond lattice (2024), arXiv:2410.13706 [cond-mat.str-el] .
18. T. Holstein and H. Primakoff, Phys. Rev. **58**, 1098 (1940).
19. D. N. Zubarev, Soviet Physics Uspekhi **3**, 320 (1960).
20. M. Newman and G. Barkema, *Monte Carlo Methods in Statistical Physics* (Clarendon Press, 1999).
21. A. M. Ferrenberg, J. Xu, and D. P. Landau, Phys. Rev. E **97**, 043301 (2018).
22. M. Campostrini, M. Hasenbusch, A. Pelissetto, P. Rossi, and E. Vicari, Phys. Rev. B **65**, 144520 (2002).
23. S. A. Kivelson, J. M. Jiang, and J. Chang, *Statistical Mechanics of Phases and Phase Transitions* (Princeton University Press, 2024).
24. B.-G. Liu, Journal of Physics: Condensed Matter **4**, 8339 (1992).
25. V. V. Mkhitaryan and L. Ke, Phys. Rev. B **104**, 064435 (2021).
26. P. M. Richards, Phys. Rev. Lett. **27**, 1800 (1971).
27. J. Kondo and K. Yamaji, Progress of Theoretical Physics **47**, 807 (1972).
28. O. Menchyshyn, T. Krokhmalskii, and O. Derzhko, Simple-cubic-lattice spin-1/2 Heisenberg model within Green-function method (2014), preprint of the Institute for Condensed Matter Physics, National Academy of Sciences of Ukraine: ICMP-14-01E .
29. S. Wessel, Phys. Rev. B **81**, 052405 (2010).

CONDENSED MATTER PHYSICS

The journal **Condensed Matter Physics** is founded in 1993 and published by Institute for Condensed Matter Physics of the National Academy of Sciences of Ukraine.

AIMS AND SCOPE: The journal **Condensed Matter Physics** contains research and review articles in the field of statistical mechanics and condensed matter theory. The main attention is paid to physics of solid, liquid and amorphous systems, phase equilibria and phase transitions, thermal, structural, electric, magnetic and optical properties of condensed matter. Condensed Matter Physics is published quarterly.

ABSTRACTED/INDEXED IN: Chemical Abstract Service, Current Contents/Physical, Chemical&Earth Sciences; ISI Science Citation Index-Expanded, ISI Alerting Services; INSPEC; "Referatyvnyj Zhurnal"; "Dzherelo".

CONTACT INFORMATION:
Institute for Condensed Matter Physics
of the National Academy of Sciences of Ukraine
1 Svientsitskii Str., 79011 Lviv, Ukraine
Tel: +38(032)2761978; Fax: +38(032)2761158
E-mail: cmp@icmp.lviv.ua http://www.icmp.lviv.ua